

Design, Fabrication, and Testing of 10 MJ Composite Flywheel Energy Storage Rotors

Authors:

1. J.D. Herbst
2. S.M. Manifold
3. B.T. Murphy
4. J.H. Price
5. R.C. Thompson
6. W.A. Walls
7. A. Alexander
8. K. Twigg

Company:

1. The University of Texas at Austin Center for Electromechanics
2. The University of Texas at Austin Center for Electromechanics
3. The University of Texas at Austin Center for Electromechanics
4. The University of Texas at Austin Center for Electromechanics
5. The University of Texas at Austin Center for Electromechanics
6. The University of Texas at Austin Center for Electromechanics
7. CAES
8. CAES

Design, Fabrication, and Testing of 10 MJ Composite Flywheel Energy Storage Rotors

J.D. Herbst, S.M. Manifold, B.T. Murphy, J.H. Price, R.C. Thompson, and W.A. Walls

Center for Electromechanics, The University of Texas at Austin

A. Alexander and K. Twigg

CAES

ABSTRACT

Flywheel energy storage systems employing high speed composite flywheels and advanced electric motor/generators are being evaluated by the Department of Defense (DoD), NASA [1], and firms [2,3] to replace electrochemical battery banks in satellites and manned space applications. Flywheel energy storage systems can provide extended operating life and significant reduction in weight and volume compared to conventional electrochemical systems. In addition, flywheels can provide momentum or reaction wheel functions for attitude control.

This paper describes the design, fabrication, and spin testing of two 10 MJ composite flywheel energy storage rotors. To achieve the demonstrated energy density of greater than 310 kJ/kg in a volume of less than 0.05 m³, the rotors utilize flexible composite arbors to connect a composite rim to a metallic shaft, resulting in compact, lightweight, high energy density structures.

The paper also describes the finite element stress and rotordynamics analyses, along with a description of the fabrication and assembly techniques used in the construction of the rotor. A description of the experimental setup and a discussion of spin testing of the rotors up to 45,000 rpm (965 m/s tip speed) are also presented. Accurate measurements of rotor centrifugal growth made with laser triangulation sensors confirmed predicted strains of greater than 1.2% in the composite rim.

Due to the weight penalty associated with flywheel designs requiring containment structures, there is a strong need to develop flywheel systems which operate safely in space, preferably without dedicated containment structures. A future paper will describe results of a 28,600 rpm composite rotor burst test performed in a containment structure as a step towards understanding composite rotor failure modes.

INTRODUCTION

Power systems subject to cyclic variations in prime power availability or needing to satisfy intermittent demands for high power may benefit from the addition of an energy storage element to reduce prime power requirements. The Center for Electromechanics (CEM) at The University of Texas at Austin has been developing high performance composite energy storage flywheels for 15 years as part of the Electromagnetic Gun Weapons System Program for the U.S. Army and, more recently, for the Defense Advanced Research Projects Agency (DARPA) Electric Vehicle Program. CEM is currently under contract to the Department of Transportation Federal Railroad Administration (FRA) to develop an advanced locomotive propulsion system (ALPS) including a composite energy storage flywheel for use in a high speed passenger locomotive application.[4]

ALPS consists of a 600 MJ flywheel energy storage system coupled to a 3 MW motor/generator and a second 3 MW high speed alternator direct coupled to a gas turbine prime mover. Figure 1 shows the power flow diagram for the locomotive propulsion system application.

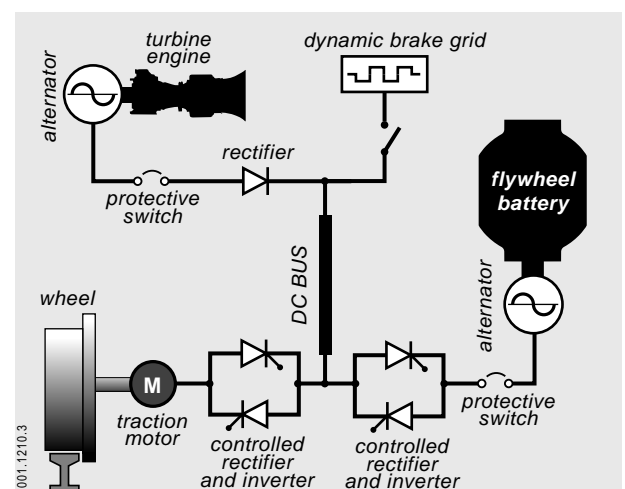


Figure 1. ALPS power flow diagram

Power from the turboalternator is fed into the locomotive DC link via a simple rectifier and is then transmitted to the AC traction motors through a bi-directional power converter. A second bi-directional power converter is used to transfer energy to and from the flywheel through the 3 MW motor/generator. A dynamic brake system is also included to resistively dissipate braking energy beyond the storage capacity of the flywheel. During acceleration and grade negotiation, prime mover horsepower is supplemented by up to 3 MW of additional power from the flywheel energy store. During deceleration and down-grade operation, braking energy can be returned to the flywheel energy store, increasing the overall propulsion system efficiency.

ALPS will allow nonelectric (fossil fueled) locomotives to match the performance of existing electric locomotives while avoiding \$1-2 million per mile electrification costs. ALPS also reduces noise and exhaust emissions compared to conventional fossil fueled locomotives. The flywheel energy storage system minimizes thermal cycling of the gas turbine, improving hot section life, and also provides significant fuel savings compared to conventional turbine powered locomotives.

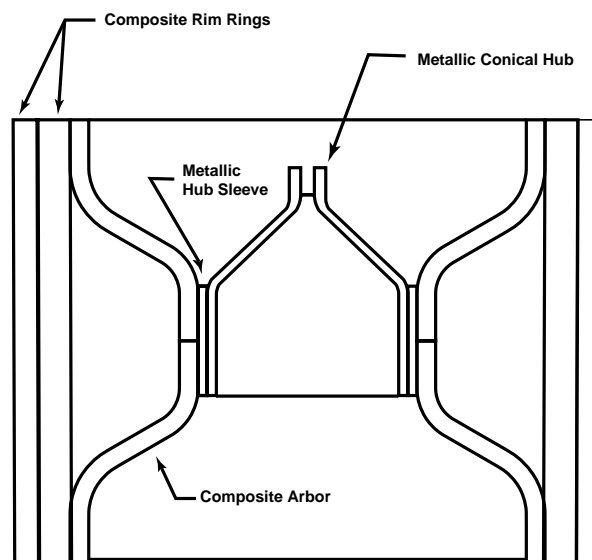
As part of the ALPS development effort, two, one-third scale composite rotors have been designed, fabricated, and tested to validate the design and analysis tools, and develop fabrication and assembly techniques for the full scale flywheel rotor. Scaling of the flywheel for the ALPS component development program was selected in part to provide a relatively simple retrofit into the flywheel energy storage system currently being developed for a mass transit bus project. This project is being conducted at under the DARPA Electric Vehicle Program with funding from the State of Texas Advanced Technology Development Program. CEM is also involved in a related contract to perform material characterization testing for qualification of composite structures for space based applications, including the International Space Station.

The unique analysis tools and fabrication techniques demonstrated in the ALPS component development program will allow the efficient design of similar composite energy storage flywheels to match a wide variety of energy storage applications, including the replacement of chemical storage batteries on space-based platforms.

FLYWHEEL DESIGN AND ANALYSIS

To maximize the specific energy of the flywheels, the rotor mass is concentrated in the composite rim, at the largest possible spin radius. The flywheels utilize lightweight, flexible composite arbors to connect the composite rim to the metallic hub assembly, resulting in compact, lightweight, high energy density structures. The rotors were configured for spin testing in a vertical orientation, with the metallic hub assembly providing the structural interface to an air turbine's quill shaft. The rotor design is

easily modified to incorporate a conventional shaft for a two bearing support configuration. Figure 2 is a cross section view of the flywheel showing the major components.



9501.0125.1

Figure 2. Cross section of flywheel

To manage radial spin stresses during operation, the flywheel rim is a hybrid of two different design approaches; radial prestress and strain matching. The flywheel rim is constructed of two concentric rings assembled with a radial interference, generating compressive radial stresses at rest to offset radial tensile spin stresses at operating speeds. To provide additional radial compression during operation, the inner ring is constructed using lower modulus, higher density materials, providing partial strain matching across the radial thickness of the rim. The trade off with the strain matched design is increased radial growth at the bore of the rim structure. The flexible composite arbors are designed to match the radial growth of the rim as well as accommodate the axial contraction of the rim.

Detailed finite element models of the flywheel composite structures and metallic hub assembly were generated to evaluate the strains in the composite structures and the loads on critical adhesively bonded joints.

STRESS/DEFLECTION ANALYSIS

Under contract to CEM, Custom Analytical Engineering Systems (CAES), of Flintstone, Maryland, performed analysis specific to the development of the composite rim and arbor assembly. The CAES proprietary pre-process

sor provides the capability to simulate ply-by-ply laminate construction of a structure, incorporating actual fabrication parameters to represent the as-fabricated component. This includes development of filament wound structures by simulating the winding process. Designs of layers forming the arbor were developed entirely by the pre-processor. Accuracy of the pre-processor has been verified by comparison with measured thicknesses of numerous pressure vessel and rocket motor case structures. The pre-processor automatically develops a unique material property description for each element in the model by determining the layer content in each element and computing the nine independent orthotropic material constants based on the strain energy contribution and orientation of every layer contained in the element. The entire finite element model description was automatically developed in the required format for transfer into the ABAQUS finite element software, including node definitions, element definitions, and material property definitions. CAES's post-processor outputs fiber path stress and strain data with graphical interpretation. Numerous iterations of the rotor design were completed to optimize stress fields for the strain matched composite arbor.

Another challenging aspect of the project was designing the means of connecting the rim and arbor to the air turbine's quill shaft. A solid disk hub was unsuitable due to the large interference required at the disk-to-arbor hub interface to prevent radial separation at high rotational speeds. Achieving the required interference presented difficult assembly problems, and the radial precompression at rest would have been high enough to drive viscoelastic response of the composite arbor hub, resulting in a possible loss of interference pressure over time. A design for a conical hub assembly constructed of high strength 4340 alloy steel was developed and analyzed by CEM.

The conical shape is much more compliant radially compared to a solid disk, allowing growth-matching of the drive hub with the arbor hub bore. Growth matching of the metallic hub to the arbor greatly reduces the interference requirements, lowering the assembly risks and radial precompression at rest.

To eliminate press fits at the arbor hub bore surface, the arbor/rim assembly was initially adhesively bonded to a cylindrical hub sleeve. Radial compression through the hub/sleeve interface and the sleeve/arbor interface was then generated by installing the conical hub into the hub sleeve bore with a tapered interference fit.

The hub structural design and the required assembly interferences were evaluated using a 1-D axisymmetric nested ring analysis and subsequent 2-D axisymmetric finite element analysis. Nested ring analysis was used to quickly provide an initial estimate of the interference required to keep the hub/sleeve and sleeve/arbor interfaces at compression at an overspeed condition. A radi-

al interference was selected resulting in a radial compression of 13.8 MPa at rest at the hub/sleeve interface, and a residual radial compression of 12.4 MPa at 47,300 rpm. Since the specific stiffness of the drive hub and sleeve is less than the arbor hub and its preload banding, the radial compression at the hub sleeve/arbor interface increases from 6.2 MPa at rest to almost 27.6 MPa at 47,300 rpm. This ensures that no separation of the drive hub from the sleeve or arbor will occur.

A 2-D axisymmetric finite element model of the metallic hub structure was constructed using PATRAN 2.5 software. The model was converted to an ABAQUS input file for processing on the University of Texas High Performance Computation Facility's Cray J-90 computer. The model was constructed of four-node linear continuum elements in a fairly refined mesh. Interface elements were used to model the assembly interferences. The finite element analysis calculated the stresses in the drive hub due to assembly interferences and operation at speeds up to 47,300 rpm. The finite element analysis was needed to accurately model the nonuniformity of the structure along the axis of rotation, especially where the drive hub transitions from a cylindrical to a conical section. In the finite element analysis, arbor structure beyond the contact length of its hub portion was ignored in order to minimize model size and computational requirements.

In general, radial and hoop stresses calculated with the finite element model agree with the stresses predicted by the nested ring analysis. Results from the two analyses diverge for stresses in the conical hub where the cylindrical section begins to slope downward to the drive shaft interface. At this point, radial stiffness of the cone is increasing, resulting in increased interference pressure between the hub and sleeve. The increased interference pressure produces a local rise in the hoop stress in the sleeve. The stress rise is not serious, however, being 951 MPa at the overspeed condition compared to 903 MPa as predicted by nested rings analysis. The highest von Mises stress in the drive hub is 779 MPa at 47,300 rpm. The highest von Mises stress in the sleeve is 930 MPa, also occurring at the overspeed condition.

ROTOR DYNAMICS ANALYSIS

In order to predict the rotordynamic behavior of the rotor during spin testing, a rotordynamics analysis was performed using TXROTOR, a finite element based code developed at CEM. Figure 3 shows the finite element (FE) rotordynamic model of the flywheel rotor, including the quill shaft used to interface with the spin test drive turbine. This model was created to verify adequate dynamic performance of the rotor in the vertically suspended configuration of the spin test. Additional rotordynamics analysis was performed on rotor configurations using conventional shaft designs. Figure 4 shows the results of the analysis of the spin test design as a plot of undamped

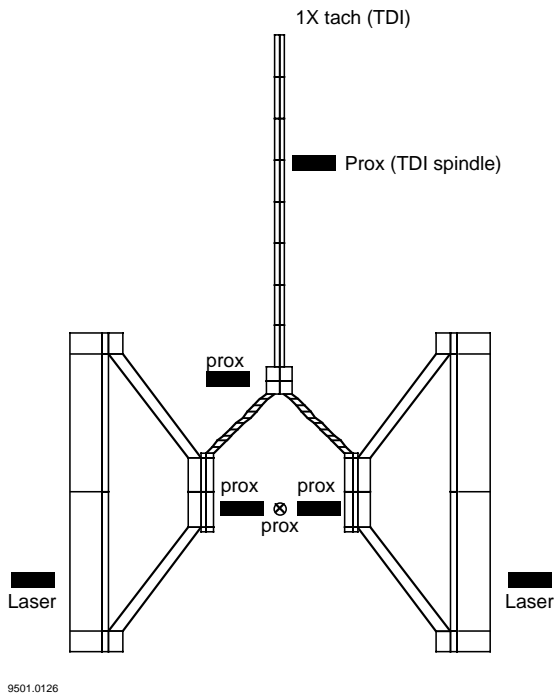


Figure 3. Rotordynamic finite element model geometry, also showing installed instrumentation

rotor natural frequencies as a function of rotor speed. Except for the two composite arbors, the FE model employs 3-node isoparametric beam elements. The stiffness properties of the arbors were determined with detailed axisymmetric and 3-D FE solid models, and input directly as an element stiffness matrix to the rotordynamic model of the flywheel rotor. The detailed 3-D analysis of the composite arbors was performed at CAES.

Gyroscopic effects are included in the analysis results presented in figure 4, and therefore there are distinct pairs of backward whirling and forward whirling rotor natural frequencies. The figure also shows three straight lines having slopes of 0.8, 1.0 and 1.2 respectively. Forward mode curves which intersect the 1.0 line define the resonant critical speeds. Thus while spinning up to 45,000 rpm, the rotor will traverse critical speeds near 250 and 24,300 rpm. These two modes can be safely traversed with the help of a vibration damper located near the midspan of the quill shaft. The damper is effective at limiting the whirling response when passing through these modes. After traversing these two modes, it is best not to traverse any more criticals at high speed, as they are more difficult to damp effectively. Thus, it is important to not have any forward modes "too close" to the 1.0 line. The 0.8 and 1.2 lines define the limits of "too close". The first forward mode to cross into the 0.8 to 1.2 range does so at 47,000 rpm. As this is above the desired 45,000 rpm maximum test speed, the rotor design was acceptable.

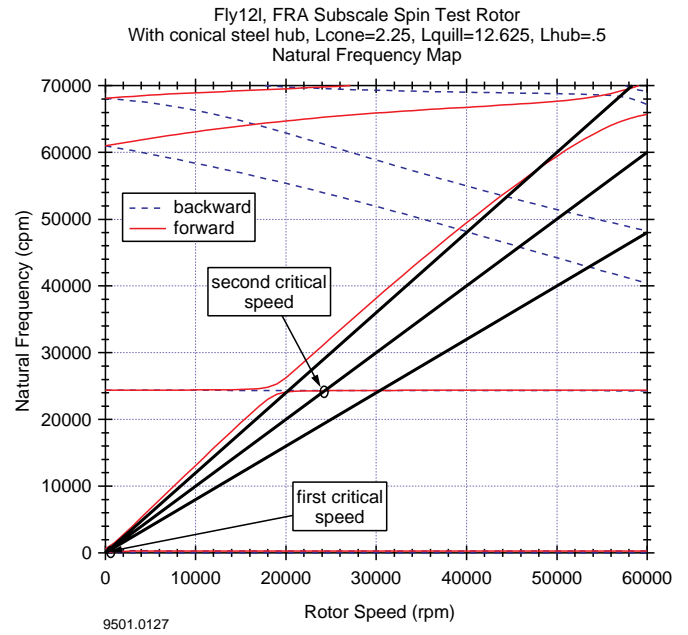


Figure 4. Rotordynamic natural frequencies of the subscale rotor as a function of rotor spin speed

FABRICATION AND ASSEMBLY

The flywheel rim and arbors are constructed using a combination of Toray M30S intermediate modulus graphite, Toray T700 standard modulus graphite, and Owens-Corning S2 fiberglass (Table 1). The resin is a Fiberite 977-2 thermosetting epoxy resin system toughened with thermoplastic additives. The composite materials were chosen as a good compromise between performance and cost, with an eye to commercial development of the full scale ALPS flywheel design. An extensive materials characterization program was conducted to develop manufacturing procedures and establish design limits for the composite materials. Additional material and component testing was performed to verify the strength of critical adhesive bonds within the flywheel. The metallic hub structure consists of a hub sleeve bonded to the composite arbors, and a conical hub providing the interface to the spin test quill shaft. Both hub components are machined from heat treated 4340 alloy steel.

The composite structures are filament wound on steel mandrels using a combination of pre-impregnated tow (towpreg) and unidirectional tape materials. The two rim rings are primarily hoop wound structures with off axis reinforcement. The composite arbors are filament wound in a four axis winding machine using multiple layers. Additional S2 towpreg material is wound onto the arbors to provide bond interfaces for the rim and support rings.

Table 1. Individual composite fiber material properties

Fiber	Number of Filaments	Tensile Strength (GPa)	Modulus (GPa)	Density (g/m ³)	Elongation* (%)
Toray T700	12,000	4.90	230	1.80	2.1
Toray M30S	18,000	5.49	294	1.73	1.7
Owens-Corning S2 Glass	N/A	4.59	86.8	2.49	5.3

* Measured using the impregnated strand test method

After winding, the composite arbors are machined to final dimensions at the interfaces to the rim and hub. The arbors are then adhesively attached with epoxy to the rim and hub using specially developed proprietary techniques. These techniques were essential to maintain favorable stresses simultaneously at both interfaces under all conditions. The two composite rim rings are assembled together with a radial interference to generate the required radial prestress. Figure 5 is a photo of the completed flywheel rotor.

SPIN TEST PROGRAM

The spin test program was conducted to validate the analysis tools used to design both full and subscale rotors. To date, a total of three experiments have been performed using two similar subscale rotors: two spin tests to assess rotordynamic and structural behavior of each rotor, and a burst test to evaluate rotor failure modes and containment structure requirements. Discussion of the burst/containment test will be in a forthcoming paper. All spin testing has been conducted at Test Devices, Inc. of Hudson, Massachusetts.



S9501.0154

Figure 5. Completed rotor

EXPERIMENTAL SET-UP

During the weeks of May 19-23 and September 15 -19, 1997, two subscale rotors were installed and tested at Test Devices. Both rotors were balanced to within 0.0127 mm of mass center offset in a Schenck vertical axis balance machine. The rotor was mounted in the balance machine with the use of a precision mandrel clamped onto the outer diameter of the steel hub at the quill insertion point. Spin testing was performed in a 100-200 millitorr vacuum inside a heavy steel containment structure. Motoring and braking power is provided by a vertical axis high speed air turbine, with the rotor suspended from the drive turbine by a 9.53 mm diameter quill shaft interference fit into the flywheel rotor conical hub. With the exception of minor modifications to the instrumentation, the experimental set-up for each spin test series was essentially identical. Figure 6 is a photo of the rotor suspended by the quill shaft from the drive turbine mounted on the lid of the spin test chamber.

After installing the rotor, an aluminum bracket was mounted to the lid of the spin test chamber to support vibration and growth monitoring instrumentation. Test instrumentation included a tachometer, several eddy current proximity probes, and a pair of laser triangulation sensors.

Measurement of rotor centrifugal growth was performed to verify the calculated stiffness and strains in the composite rim and arbor structures. During the first test series, two eddy current probes and two different laser triangulation systems were used to monitor radial growth on the outside diameter of the graphite rim. Based on results from these tests, only the IDEC laser triangulation system was used during the second test series. In-pit audio and video monitoring were also added during the second test series. Additional eddy current proximity probes monitored the dynamic position of the metallic hub structure of the rotor, both inside the conical hub and at the outside diameter near the quill shaft attachment point. In addition to these sensors, an eddy current proximity probe monitored the vibration of the quill shaft, and a one-per-rev tachometer signal monitored rotor speed and phase angle.

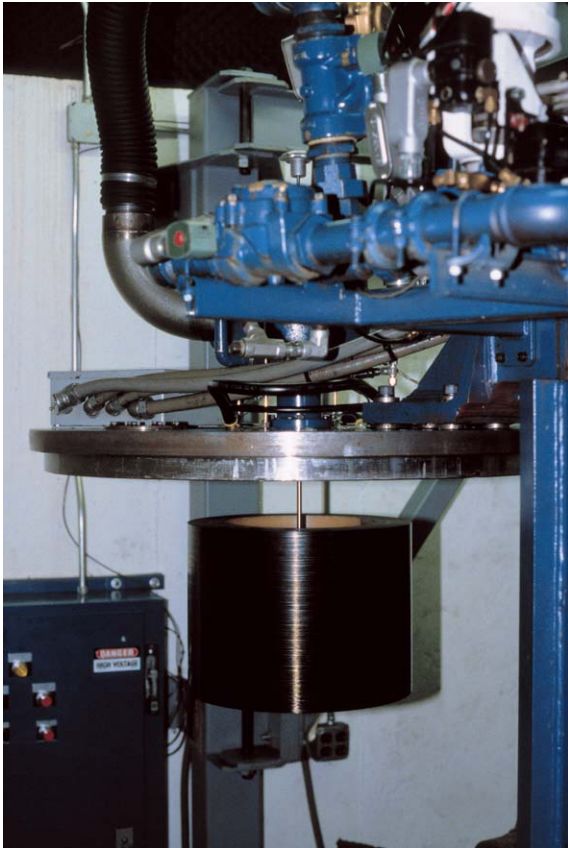


Figure 6. Rotor on lid of spin pit

Table 2. Subscale rotor spin test speeds

Test Speed (rpm)	Calculated Strain (%)	Tip Speed (m/s)
25,300	0.45	544
31,000	0.60	667
35,300	0.75	760
39,500	0.90	852
43,200	1.05	933
45,000	1.13	973

Vibration, rotor growth, and tachometer data generated during each test run was collected and monitored on a Zonic[®] WCA digital signal analyzer.

SPIN TEST 1

Prior to spin testing, the natural frequencies and mass balance of the rotor were measured. In both the full scale and subscale rotors, the maximum speed (and stored energy) of the rotor is dictated by the need to maintain approximately 20% margin between the operating speed frequency and any natural frequencies of the rotor structure. In both subscale and full scale rotors, the limiting natural frequency is defined by the “arbor mode”, a vibration mode characterized by relative motion between the mass of the rim and the mass of the shaft/hub structures. The frequency of the arbor mode is controlled by the lateral stiffness of the composite arbors. The fundamental arbor mode frequency predicted by finite element analysis was approximately 1 kHz. The corresponding measured natural frequency for the subscale rotor was approximately 1.3 kHz, indicating that the lateral stiffness of the composite arbors is slightly higher than was predicted.

Spin test speeds of the subscale rotor were selected to demonstrate strains equivalent to those present at selected energy storage levels in the full scale machine. Table 2 shows the subscale spin test speeds, and calcu-

lated strain levels in the rim. The relatively large strains and corresponding radial growth experienced by the rotor rim, make balance retention and repeatability a critical characteristic. Multiple runs were performed to each test speed to evaluate retention of rotor mass balance.

During the first spin test series 10 tests were performed: one check-out test to 10,000 rpm, three tests to 25,300 rpm, three tests to 31,000 rpm, two tests to 35,300 rpm, and a maximum speed of 39,500 rpm achieved during the final test. Vibration and rotor growth data were examined between each run to look for changes in the rotor-dynamic behavior of the rotor and to correlate measured and predicted rotor growth values. A visual inspection of the rotor and instrumentation was also done between tests.

After the first planned test to 39,500 rpm, a visual inspection of the rotor revealed a partial unbond of the adhesive bond between a mass-loading layer and the inner surface of the arbor. Because of the shift in vibration characteristics (discussed below) and the danger of a large, uncontrolled shift in rotor balance if this adhesive bond separation propagated, testing was stopped at this point.

After return to CEM, a computerized axial tomography (CAT) scan was performed to examine the internal structure of the rotor. The CAT scan revealed a hoop failure of a small region in an S2 glass layer just inboard of the rim/arbor interface bond, which could account for the shift in rotor dynamic behavior during the test to 31,000 rpm. This material is part of glass layers used only to create the interface for the rim/arbor adhesive bond, and was eliminated during construction of the second subscale test rotor.

For testing of the first rotor, two different laser triangulation sensors were used (fig. 3). One made by Aromat with a 50 ms response time, and the other by IDEC with

a 1 ms response time. The response time of the Aromat apparently was too slow, so its data is not presented. Static calibrations of eddy current sensors on the composite rim were promising, but signals from the spinning rotor were clearly useless. Figure 7 shows the filtered synchronous components measured on the last test by eddy current sensors on the steel quill and hub, and the IDEC laser looking at the rim outer diameter. By virtue of the flexible quill shaft, at speeds above 1000 rpm mass center inversion has taken place, and the rotor essentially spins about its inertial center. So then the “low speed” runout (< 5,000 rpm) of the hub is seen to be just 5 μm . This means the geometric center of the hub’s inner surface is 5 μm from the rotor mass center. Likewise, the outer surface of the rim is seen to be about 15 to 20 μm from the mass center. Given the tolerances adhered to during fabrication and assembly, these runout values are considered quite small.

The traces in figure 7 show that just above 35,000 rpm the vibration begins changing abruptly. As mentioned earlier, testing was halted after this run, and post test inspections revealed debonding of both a mass-loading layer and sacrificial S2 glass material internal to the rotor.

There is very little published data for centrifugal growth of composite rotors [5]. Figure 8 shows the centrifugal growth of the composite rim as measured by the laser sensor. The anticipated quadratic nature of the data is clearly evident. The measured growth at 39,500 rpm is 1.46 mm radial (57.6 mils). The predicted growth from the 1D nested ring analysis is 1.40 mm (55.0 mils), for a

difference of 4.7%. The laser was carefully calibrated with a gap resolution of about 5 μm , but with a static setup. Overall, the measured centrifugal growth is believed to be accurate to $\pm 13 \mu\text{m}$ (0.5 mils).

SPIN TEST 2

The second subscale rotor was built and tested to evaluate design and assembly procedure modifications implemented to address problems experienced during spin testing of the first subscale rotor. These modifications included changes to the geometry of the sacrificial glass layers at the rim/arbor interface, and improved surface preparation techniques used in bonding the mass-loading layer to the inner surface of the composite arbor. Further evaluation of rotor growth instrumentation was also performed.

A total of 14 tests were performed: one check out test to 10,000 rpm, two tests to 25,300 rpm, three tests to 31,000 rpm, three tests to 35,300 rpm, three tests to 39,500 rpm, one tests to 43,200 rpm, and a maximum speed of 45,000 rpm achieved during the final two tests. Vibration and rotor growth data were examined between each run to look for changes in the rotordynamic behavior of the rotor, and to correlate measured rotor growth with predicted values.

The test runs were uneventful until the first run to 39,500 rpm. During this test, starting at approximately 36,500 rpm, quill shaft vibration began to increase. The test was

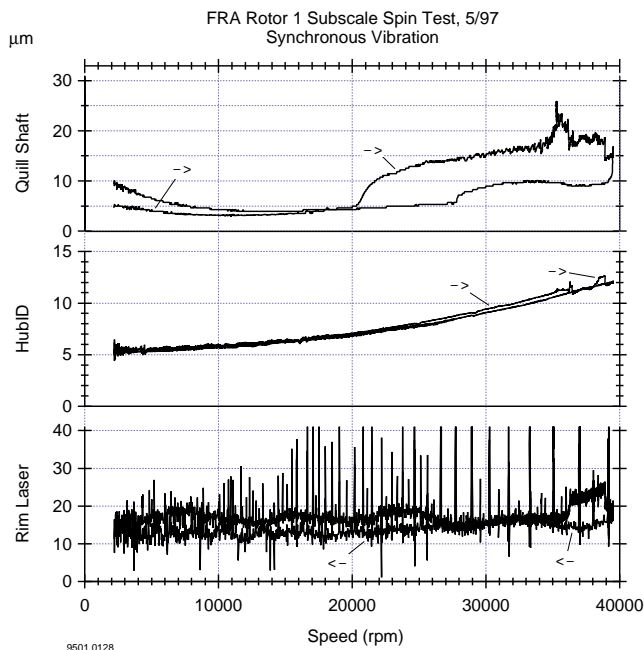


Figure 7. Synchronous vibration from the last run of rotor 1 to 39,500

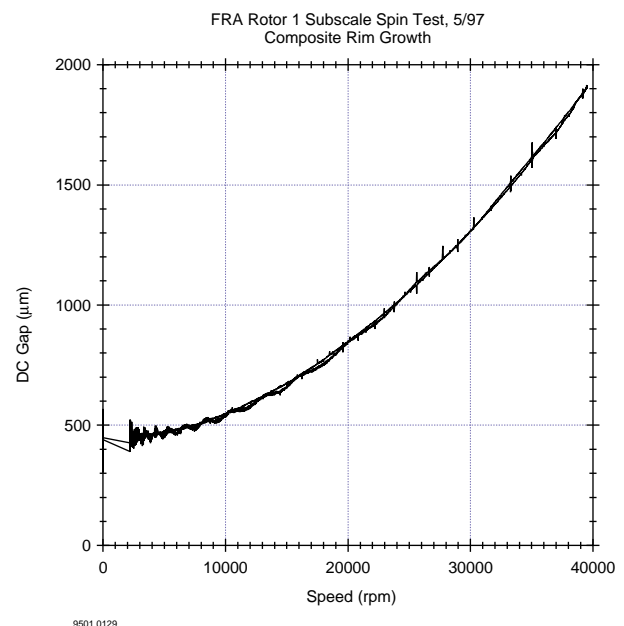


Figure 8. Static gap data from the IDEC laser sensor on the last run of rotor 1 to 39,500 rpm

halted at 37,169 rpm as the quill shaft vibration amplitude had grown rapidly from 0.0064 mm to 0.0381 mm (zero-to-peak). The spin chamber was opened to inspect the rotor, which revealed superficial cracks in the thick epoxy layer on the inner surface of the arbors, particularly in the region of the lower blend radius adjacent to the hub. The cracks were oriented axially and did not extend into the fiber reinforced regions of the arbor structure. A review of the stress analysis results in this region indicated relatively low transverse stresses, indicating this may be a resin “crazing” phenomenon, a relatively benign situation. Zonic digital signal analyzer traces collected during braking indicated a permanent shift in the rotor mass center of approximately 0.0254 mm. This implied that a permanent change had occurred in the rotor structure. Examination of the stresses at this speed indicated that the mass center shift may have been caused by relief of residual axial stresses between the metallic conical hub and metallic hub sleeve. The mass center shift did not appear attributable to the composite arbor or rim.

Two additional tests to 39,500 rpm were then performed. Vibration traces taken during these tests retraced the vibration signals collected during deceleration during the test to 37,169 rpm. Visual inspections after each test revealed no propagation of the cracks observed in the epoxy layer on the inner surface of the arbors, but the number of cracks increased after each test. After the second successful test to 39,500 rpm, an unbond of the adhesive between the mass-loading layer and the inner surfaces of the arbors had begun. The appearance of the composite surface and the relatively low shear stresses in this region point to continued problems with the surface preparation procedure. Because these mass-loading layers are more critical for long term fatigue performance, testing was allowed to continue as long as the partially separated mass-loading material did not significantly affect rotor balance.

In order to accelerate the test sequence only one test was performed to 43,000 rpm before proceeding to the 45,000 rpm tests. The test to 43,000 rpm was uneventful and the visual inspection after the test revealed no propagation of the cracks in the epoxy layer on the inner surface of the arbor.

The first 45,000 rpm test run was successful, with no significant increase in the vibration levels. At this speed, the strains in the subscale rim and arbor structures match the calculated strains in the full scale rotor at a speed corresponding to 600 MJ of energy storage.

During the second test to 45,000 rpm, a shift in the rotor orbit and an abrupt increase in quill shaft vibration of 0.0076 mm occurred at 43,678 rpm. Acceleration continued to 44,968 rpm when the test was terminated. Inspection of the rotor revealed strings of graphite material had separated from the outside diameter of the rim. The composite material separated around the entire circumference of the rim and extended approximately 5 mm

from the end face of the rotor and approximately 0.76 mm deep. Subsequent analysis indicates that unbalanced forces created by balance correction weights led to bending stresses which added to the centrifugal strains at the outer surface of the rim. This information will be used to modify the techniques for balance correction in the full scale rotor.

For testing the second rotor the Aromat laser sensor was replaced with another IDEC, 180 degrees opposite the first. This allows a more accurate measurement of the growth $[(s1+s2)/2]$ and offset $[(s1-s2)/2]$ of the outer surface of the rotor. Also another eddy current sensor was added at the hub bore to enable monitoring and display of rotor orbits.

Figure 9 shows vibration data from the last run, to 45,000 rpm. The slow speed runouts inside the hub and outside the rim are considerably larger than for the first test rotor. The steel hub runout is about 90 μm (3.5 mils), and the rim is about 260 μm (10.2 mils). These runout values are probably more typical than those from the first test rotor.

Figure 9 shows that during acceleration, at 43,678 rpm, an abrupt change occurred in hub runout of about 10 μm (0.4 mils). At this same instant, the signal from one IDEC laser was lost. Apparently, the missing band of composite material mentioned earlier came off at this time, causing the runout to change and cut the lead to the IDEC (found during post test inspection).

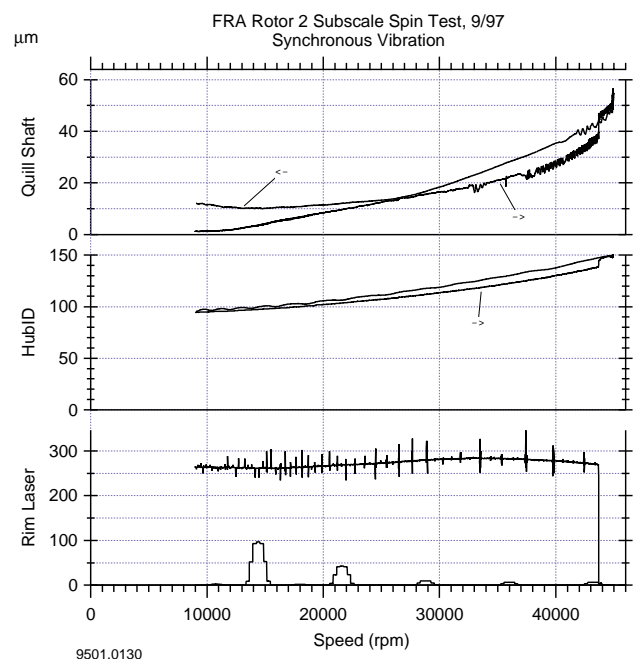


Figure 9. Synchronous vibration from the last run of rotor 2 to 45,000 rpm

Figure 10 shows the centrifugal growth measured by one of the IDEC laser triangulation sensors. Again, the expected quadratic nature of the data is clearly evident. By averaging the static gap data from both transducers, the effect of rotor offset, should any occur, is eliminated. In this fashion the measured growth at 45,000 rpm was determined to be 1.80 mm (71.0 mils). This compares favorably with the predicted value of 1.81 mm (71.3 mils) for a difference of just 0.4%. An important result here is the implication that rotor strain, and thereby rotor stress, can be predicted with similar confidence. For flywheel battery systems designed without bulky burst containment structures, accuracy of stress analysis is crucial.

Overall, until the strip of composite came off, the vibration behavior of the rotor was excellent, varying only slightly from run to run. While the rotor outer diameter grew as much as 1.80 mm, changes the rotor runout were generally on the order of 0.003 mm, or less. During many runs there was no measurable change in runout. These are very encouraging results in light of findings of other researchers [6].

CONCLUSIONS

The Center for Electromechanics, in conjunction with Custom Analytical Engineering Systems, has developed effective design and analysis tools for the evaluation of high performance energy storage rotor designs utilizing flexible composite arbors to connect the composite rim to the shaft structure.

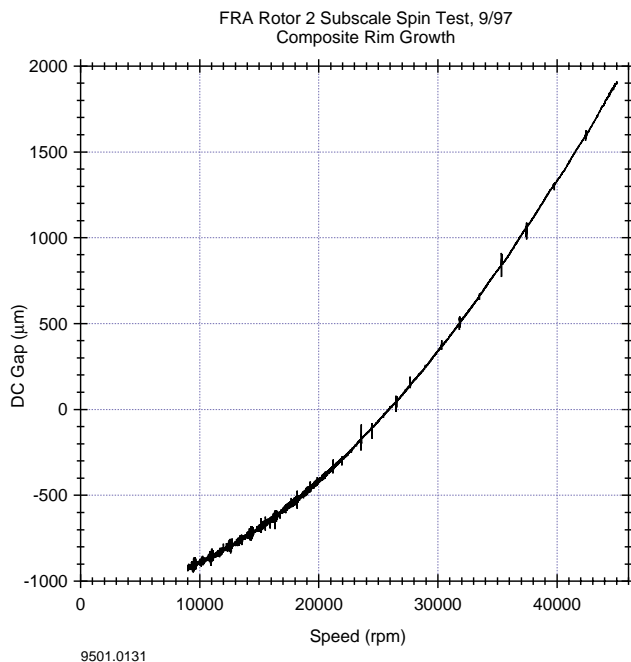


Figure 10. Static gap data from one laser sensor for the first run of rotor 2 to 45,000 rpm

Analysis accuracy has been validated with spin test results showing excellent agreement with the calculated values of rotor growth and strain (4.7% and 0.4% errors for the two test rotors). These tools can also be used to evaluate rotor designs using multiple nested arbors to increase the strength and stiffness of the rim/arbor connection.

The subscale rotor test program allowed the development of fabrication and assembly techniques to achieve the required interface conditions specified by the design analysis. These techniques were developed with construction of the full scale ALPS rotor in mind, and are thus applicable to rotor designs over a wide range of sizes.

The test program also developed instrumentation and diagnostic tools used to monitor the performance of the rotor during operation and provide information about the structural condition of the rotor after testing.

The laser triangulation sensor made by IDEC with a 1 ms response time allowed accurate measurement of rotor radial growth during spin testing to 45,000 rpm. This provides a direct measurement of strains in the composite structures. A laser with a 50 ms response time, made by Aromat, did not work well for this particular application.

The use of Computerized Axial Tomography (CAT) scanning proved to be an extremely useful tool for inspection of the internal structure of the assembled rotor.

The Center for Electromechanics is currently a participant with the NASA and U.S. Airforce Space Based Flywheel Development Program to advance composite materials development and qualify specific composite material systems for use in space applications. This program will perform additional composite materials characterization work, with a primary focus on long term fatigue behavior.

ACKNOWLEDGMENTS

Work reported in this paper was performed under the sponsorship of the U.S. Department of Transportation Federal Railroad Administration, the State of Texas Match Pool, the Defense Advanced Research Projects Agency (DARPA), and the Southern Coalition for Advanced Transportation (SCAT).

CONTACT

Mr. John Herbst
 Center for Electromechanics
 The University of Texas at Austin
 PRC, Mail Code R7000
 Austin, TX 78712
 (512) 471-4496 Fax (512) 471-0781
 j.herbst@mail.utexas.edu

REFERENCES

1. D.A. Christopher and R. Beach, "Flywheel Technology Development Program for Aerospace Applications," 1997 IEEE.
2. T.J. Pieronek, D.K. Decker, and V.A. Spector, "Spacecraft Flywheel Systems -- Benefits and Issues," 1997 IEEE.
3. J. Edwards, D.A.Christopher, J.W. Aldrich, R.F. Beach, and J.R. Barton, "Flight Test Demonstration of a Flywheel Energy Storage System on the International Space Station," 1997 IEEE.
4. T. Tsai and J. Price, "Advanced Non-Electric Propulsion System for High Speed Rail."
5. R.S. Steele and E.F. Babelay, Jr., "Data Analysis Techniques Used at the Oak Ridge Y-12 Plant Flywheel Evaluation Laboratory," Proceedings of the 1980 Flywheel Technology Symposium, Scottsdale, AZ, p 423-433.
6. R.S. Steele, "Composite Flywheel Balance Experience," Proceedings of the 16th Intersociety Energy Conversion Engineering Conference, Atlanta GA, August 1981.